JACS Au
AN OPEN ACCESS JOURNAL OF THE AMERICAN CHEMICAL SOCIETY

pubs.acs.org/jacsau
Article

Extracellular Vesicle Spherical Nucleic Acids

Hao Chen,[⊥] Qiaojiao Ding,[⊥] Lin Li, Pengyao Wei, Zitong Niu, Tong Kong, Pan Fu, Yuhui Wang, Jiang Li,* Kaizhe Wang,* and Jianping Zheng*

Cite This: *JACS Au* 2024, 4, 2381−2392
Read Online

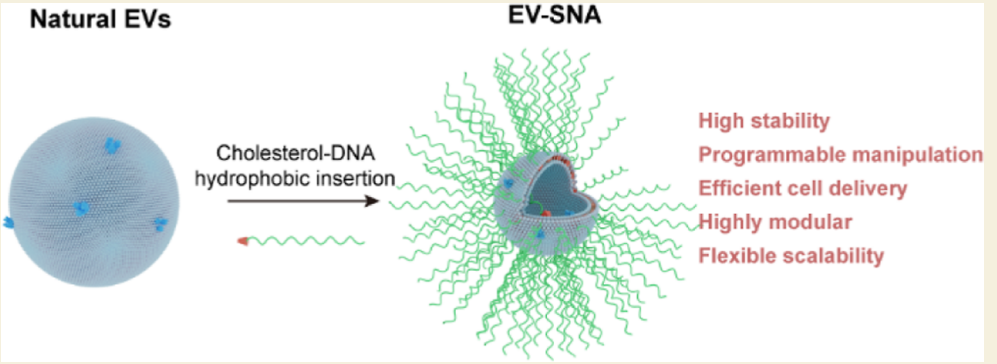

ABSTRACT: Extracellular vesicles (EVs) are naturally occurring vesicles secreted by cells that can transport cargo between cells, making them promising bioactive nanomaterials. However, due to the complex and heterogeneous biological characteristics, a method for robust EV manipulation and efficient EV delivery is still lacking. Here, we developed a novel class of extracellular vesicle spherical nucleic acid (EV-SNA) nanostructures with scalability, programmability, and efficient cellular delivery. EV-SNA was constructed through the simple hydrophobic coassembly of natural EVs with cholesterol-modified oligonucleotides and can be stable for 1 month at room temperature. Based on programmable nucleic acid shells, EV-SNA can respond to AND logic gates to achieve vesicle assembly manipulation. Importantly, EV-SNA can be constructed from a wide range of biological sources EV, enhancing cellular delivery capability by nearly 10−20 times. Compared to artificial liposomal SNA, endogenous EV-SNA exhibited better biocompatibility and more effective delivery of antisense oligonucleotides in hard-to-transfect primary stem cells. Additionally, EV-SNA can deliver functional EVs for immune regulation. As a novel material form, EV-SNA may provide a modular and programmable framework paradigm for EV-based applications in drug delivery, disease treatment, nanovaccines, and other fields.

KEYWORDS: *extracellular vesicles, exosomes, spherical nucleic acids, DNA nanotechnology, cellular delivery*

1. INTRODUCTION

The design and reconstruction of endogenous substances enable the creation of new materials with unprecedented properties, offering unparalleled promise for biomedical applications. Extracellular vesicles (EVs) are nanoscale membrane-bound vesicles that are secreted by almost all types of cells, enabling the horizontal transfer of various bioactive molecules to mediate intercellular communication.[1] Compared to synthetic nanoparticles, EVs as naturally occurring vesicles possess evolutionary selection advantages, rendering them attractive alternative vehicles for cargo delivery. EVs have excellent biocompatibility, desired nanoscopic size, low immunogenicity, and the ability to overcome biological barriers.[2,3] The remarkable features of EVs enable them to deliver endogenous functional components as well as to carry exogenous drugs, driving the development of EV-based therapies and bioengineering.[4−6] However, the full potential of EVs has not yet been realized, mainly due to their poor controllability and limited cellular delivery capacity.

Researchers have made extensive efforts to modify EVs to transform them into controllable and efficient delivery vehicles. For example, to increase the stability of EVs, supramolecular complexes and polymers have been introduced onto the vesicle surface for EV encapsulation.[7,8] However, while this improves the structural stability of EVs, it also limits their subsequent cellular delivery applications. To improve the cellular delivery efficiency of EVs, some targeting moieties, such as proteins,[9] cell-penetrating peptides,[10] targeting peptides,[11,12] aptamers,[13,14] and magnetic nanoparticles,[15] have been modified on the EV surface to improve their cellular delivery capability.

Received: April 16, 2024
Revised: May 16, 2024
Accepted: May 17, 2024
Published: May 30, 2024

https://doi.org/10.1021/jacsau.4c00338
JACS Au 2024, 4, 2381−2392

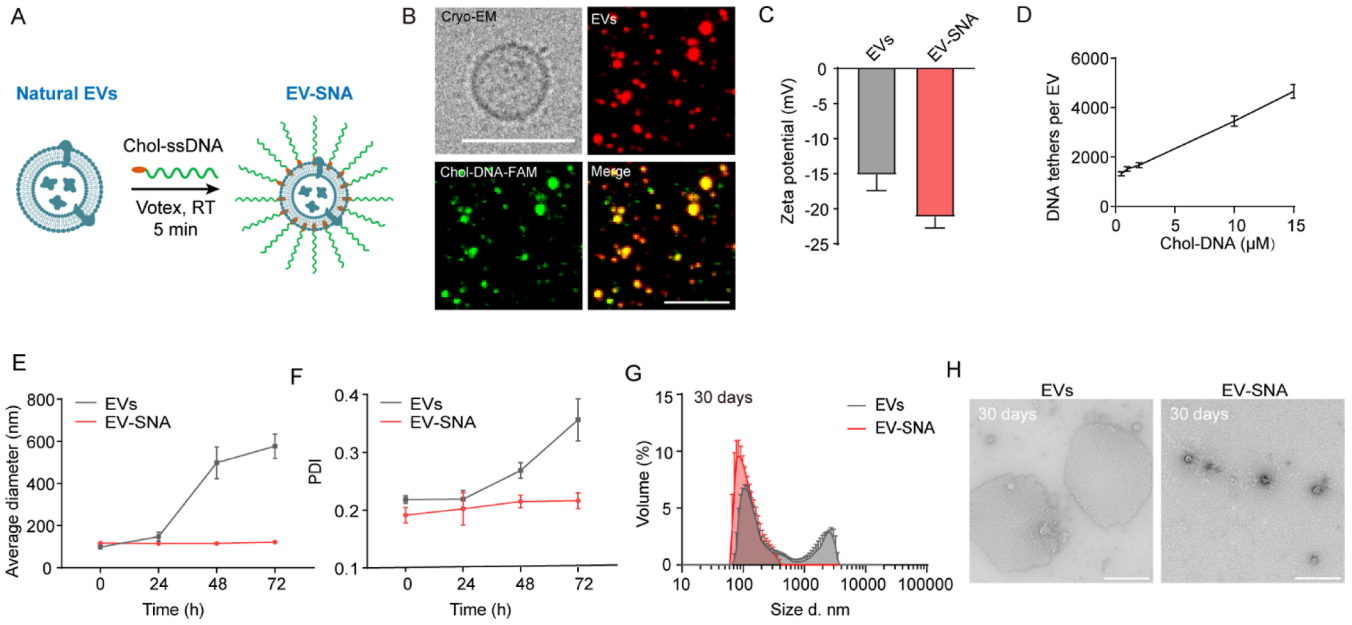

Figure 1. Characterization and enhanced stability of EV-SNA. (A) Schematic illustration of EV-SNA prepared by simply shaking EVs and cholesterol-oligonucleotide (Chol-DNA). (B) Cryo-EM image of EVs (scale bar, 100 nm), and total internal reflection fluorescence microscopy (TIRFM) images (scale bar, 5 μm) of EVs deployed with FAM-Chol-DNA. EVs were stained with red membrane dye. (C) Zeta potentials of EVs and EV-SNA. Data were presented as mean ± SD (n = 3). (D) Average amount of DNA on the single EV at different Chol-DNA concentrations. (E, F) Change in average diameter and polydispersity index (PDI) of EVs and EV-SNA after 72 h at room temperature. (G, H) Size distribution and transmission electron microscopy (TEM) images of EVs and EV-SNA after 30 days at room temperature. Scale bar, 500 nm.

However, these moieties provide only a limited improvement in delivery efficiency and have inherent problems in maximizing their functional applications, such as complex and cumbersome operations, unsatisfactory modification efficiency, poor accessibility, and lack of scalability. Furthermore, the majority of EV modifications are personalized strategies based on specific cell types or vesicle properties,[16] and the complex heterogeneity of EVs renders these customized strategies lacking in universality.[17−19] Most importantly, almost all engineered EV strategies are based on the introduction of a specific functional group to enhance a single property, often neglecting or even weakening other EV features, thus lacking a comprehensive solution. Hence, there is an urgent need to develop a novel framework paradigm for EVs to achieve enhanced overall properties and robust EV manipulation.

Spherical nucleic acids (SNAs) represent a distinctive and well-characterized nanostructure invented by Mirkin et al.[20] They are characterized by a highly oriented, dense arrangement of oligonucleotides (DNA or RNA sequences) on a spherical core, forming a three-dimensional extended nanostructure.[21] The three-dimensional structure of SNAs enables efficient cellular uptake without the need for transfection agents[22] and facilitates codelivery of other functional payloads,[23,24] providing a new paradigm for the programmable design of nanoparticles. Various synthetic materials such as molecules,[25] gold nanoparticles,[26] polymers and liposomes,[27−29] and so forth and some endogenous components such as β-galactosidase[30] and Cas9,[31] have been used to construct SNAs that enable efficient delivery of chemicals, proteins, nucleic acids, and vaccines. However, the solid core in artificially synthesized SNAs limits drug loading, and polymers and enzymes are personalized customization, while liposomes present inherent biosafety risks.[32] Therefore, there is an urgent need to explore a new generation of functional cores with high biocompatibility and versatility.

In this study, we develop a class of versatile extracellular vesicle spherical nucleic acids (EV-SNA) by simple coassembly of natural nanovesicles with cholesterol-modified oligonucleotides. We find that EV-SNA displays remarkable stability, maintaining integrity at room temperature for up to 30 days. The programmable nucleic acid sequence allows us to assemble EV-SNA with AND gate logic operations. Importantly, EV-SNA significantly enhances cell delivery efficiency by 10−20-fold. Furthermore, EV-SNA displays unique modularity and can be tailored to EVs from diverse biological sources. Compared to synthetic liposomal SNAs, endogenous EV-SNA exhibits superior antisense oligonucleotide (ASO) delivery efficiency in hard-to-transfect primary MSCs. In addition, EV-SNA is capable of delivering functional EVs for immune modulation in macrophages.

2. RESULTS AND DISCUSSION

2.1. Fabrication and Characterization of EV-SNA

In our design, the EV-SNA consists of a modularized structure with internal endogenous EVs from various biological sources and an outer layer of programmable single-stranded (ss-) DNA. The cholesterol-modified ssDNA (chol-DNA) is coincubated with EVs, and through simple vortex oscillation for 5 min at room temperature, the oligonucleotide can efficiently insert into the vesicle phospholipid bilayer via hydrophobic interactions, forming a three-dimensional dense extended structure on the vesicle surface (Figure 1A).

First, we selected EVs derived from the human breast cancer cell line MDA-MB-231 as the experimental model to construct EV-SNA. EVs were isolated from the serum-free culture medium via a series of ultracentrifugation steps. The TEM and nanoparticle tracking analysis results revealed that EVs exhibited a typical spherical or cup-shaped structure, with a size distribution ranging from 100 to 200 nm, confirming the

https://doi.org/10.1021/jacsau.4c00338
JACS Au 2024, 4, 2381−2392

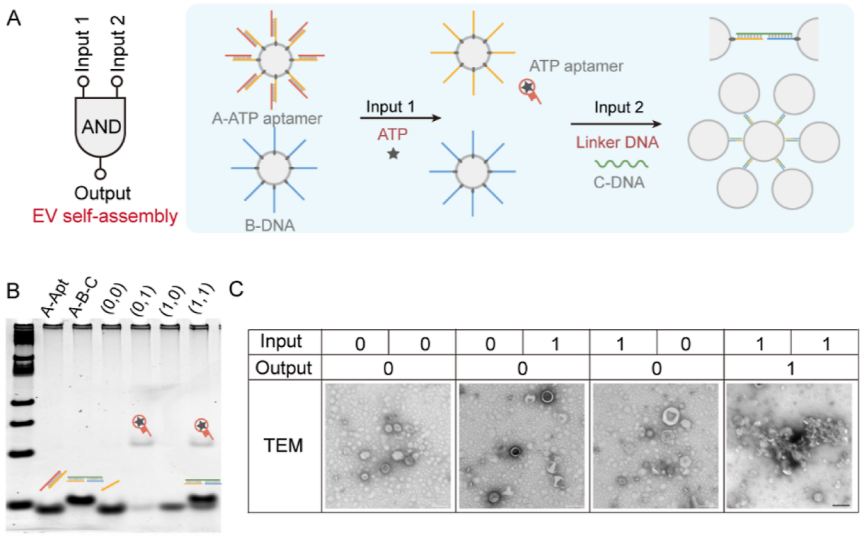

Figure 2. DNA-programmed AND logic-gated assembly of EV-SNA. (A) Schematic illustration of the DNA-directed EV assembly in response to conditional AND logic gates. (B) Gel electrophoresis analyses of mixtures in response to different external inputs. (C) TEM images of EVs under different input conditions. Conditions: without linker DNA or ATP (0, 0), with ATP (0, 1), with linker DNA (1, 0), with both linker DNA and ATP (1, 1). Scale bar, 100 nm.

successful extraction of EVs (Figure S1). Under cryo-EM, EVs exhibited a circular lumen membrane structure of around 100 nm in diameter (Figure 1B). Next, we evaluated the feasibility of these cholesterol-modified oligonucleotides (random sequence, 21 nt) for EV surface engineering to construct EV-SNA. The EVs were coincubated with FAM-labeled chol-DNA (10 μM) for 5 min with gentle shaking (600 rpm) or stationary incubation. Subsequently, the unbound chol-DNA was removed by centrifugation in a 100 kDa ultrafiltration tube. Compared to the stationary incubation group, the gentle shaking group showed a significant increase in the fluorescence signal (Figure S2A). We subsequently chose the gentle shaking condition (600 rpm, 5 min) for constructing the EV-SNA. By using TIRFM, we observed FAM fluorescence was well colocalized with the fluorescence emitted from the EV membrane red dye (Figure 1B), suggesting effective decoration of the chol-DNA on the EV membranes. After modification with chol-DNA, there was a significant decrease in the zeta potential from −15.2 to −21.2 mV (Figure 1C). Dynamic light scattering (DLS) analysis showed a significant increase in particle size after EV modification by chol-DNA (Figure S2B). To exclude the possibility of nonspecific adsorption of DNA to EVs, we coincubated chol-modified and unmodified DNA (both were labeled with FAM) with EVs and removed unbound DNA through ultrafiltration. The multimode reader results showed a strong FAM fluorescence signal only in the chol-modified oligonucleotide group, indicating that DNA was inserted into EVs through cholesterol hydrophobic modification (Figure S2C). Next, we calculated the number of oligonucleotide insertions on individual EVs by fluorescence intensity calibration. We found that the number of DNA strand insertions on EV membranes increased proportionally with the initial chol-DNA concentration. As the chol-DNA incubation concentration increased from 0.5 to 15 μM, the average number of DNA that could increase from approximately 1320 to 4660 DNA strands per vesicle, reaching 3453 ± 206 DNA strands per vesicle at a reaction concentration of 15 μM (Figure 1D). Taken together, these results collectively indicate the feasibility of constructing a dense three-dimensional nucleic acid shell on the surface of endogenous EVs through hydrophobic insertion, offering a simple approach to build an EV-SNA nanostructure.

The degradability and instability of native EV structures severely limit their utility.[8,33] Next, we analyzed the stability of the EV-SNA configuration. Both native EVs and EV-SNA were positioned in PBS at room temperature. DLS measurement data showed that storage of native EVs for 3 days resulted in a broad size distribution profile with an increase in mean particle size and PDI (Figures 1E,F and S3A), which implies the rupture or fusion of EVs. The TEM images also indicated the formation of large polydisperse structures in this group (on average > 100 nm structures with some microsized entities) (Figure S3B). In sharp contrast, EV-SNA exhibited a preserved uniform size distribution profile after 30 days of storage under almost identical conditions, a conclusion further confirmed by TEM imaging (Figure 1G,H). These results indicate that the EV-SNA construct exhibits exceptional stability.

2.2. DNA-Programmed EV-SNA Manipulation

The programmable DNA provides unparalleled controllability to nano materials, such as the ability to bind complementary nucleic acids and undergo condition-responsive conformational changes.[34−36] An important property of EV-SNA is its ability to cooperatively bind complementary nucleic acids, providing EV-SNA with programmable manipulation capabilities. To determine this, EV-SNA was coincubated with matched or unmatched FAM-DNA. We observed only a minimal fluorescence signal in the unmatched DNA group, possibly due to residual fluorescently labeled oligonucleotides. However, there was a significant increase in the fluorescence signal in the matched group, suggesting that the nucleic acids on the surface of EV-SNA retain specific binding capabilities (Figure S4). Based on this, we constructed a DNA-programmed AND logic-gated assembly of EV-SNA. In the construction of the AND logic gate module, EV surfaces were functionalized with A-DNA, designed to bind to an ATP aptamer through complementary base pairing and dissociate in the presence of ATP. Another set of EVs was functionalized with B-DNA. A linker sequence, C-DNA, complementary to the oligonucleotide sequences of both A-DNA and B-DNA, was utilized to facilitate assembly through

https://doi.org/10.1021/jacsau.4c00338
JACS Au 2024, 4, 2381−2392

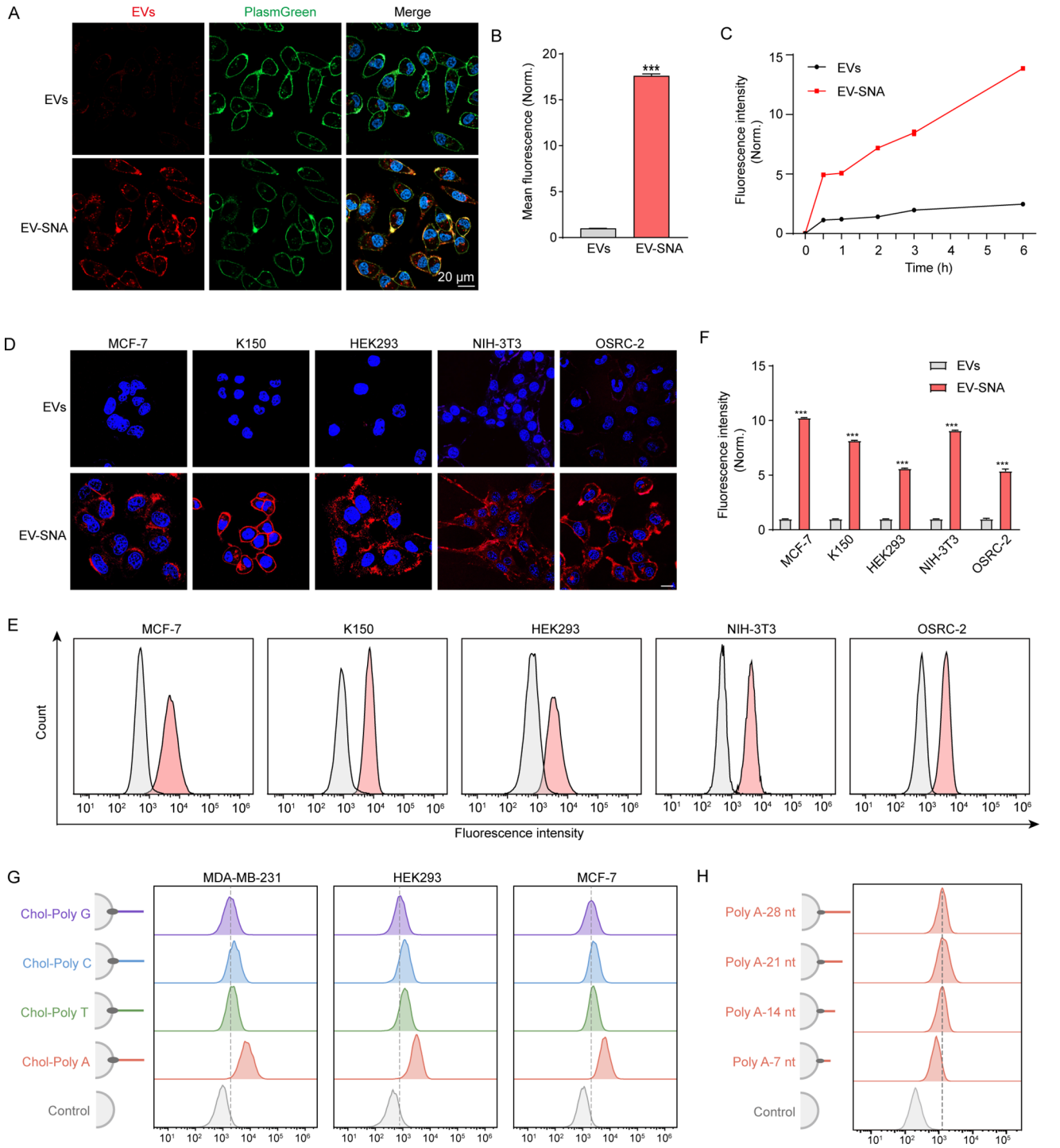

Figure 3. Programmable cellular uptake of EV-SNA. (A) Confocal images show cellular uptake of EV-SNA in MDA-MB-231 cells after 3 h of incubation. EVs were labeled with red membrane dye. Cells were stained with PlasmGreen dye. (B) Flow cytometric assay and quantification of the EV-SNA fluorescence levels in MDA-MB-231 cells. (C) Cell uptake kinetics curve of EV-SNA. (D–F) Confocal images and flow cytometric analysis of MCF-7, K150, HEK293, NIH-3T3, and OSRC-2 cells incubated with EV-SNA derived from MDA-MB-231 after 3 h incubation. EVs were stained with red membrane dye. Cell nuclei were stained with Hochst33342. Scale bar, 20 μm. (G) Uptake of EV-SNAs modified with different oligonucleotide sequences. (H) Flow cytometric quantification of EV-SNA uptake constructed with Chol-Poly A with different lengths. Data were represented as mean ± SD ***$p < 0.001$, by Student's t test.

hybridization. When ATP and C-DNA are simultaneously input into the system, it triggers the operation processing, leading to the self-assembly of EV-SNA as the output signal (Figure 2A). We first characterized the feasibility of the experimental design by gel electrophoresis. The change in band migration was only observed when both ATP (input 1) and the linker C-DNA (input 2) were present, indicating the formation of the AND gate product (lane 7) (Figure 2B). These results provide the possibility for the following logical assembly of vesicle surface biocomputing operations. As shown in Figure 2C, when a single input signal was present, EV-SNA exhibited a dispersed state. However, when both ATP and linker C-DNA were simulta-

https://doi.org/10.1021/jacsau.4c00338
JACS Au 2024, 4, 2381−2392

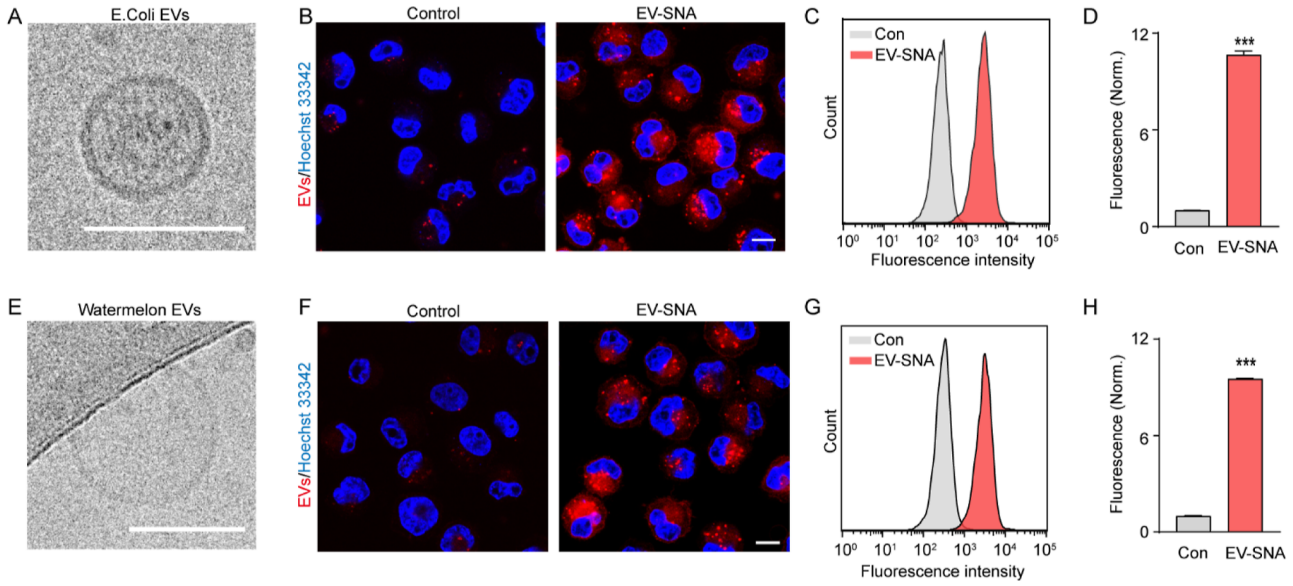

Figure 4. EV-SNAs were constructed by EVs of different biological sources. (A, E) Cryo-EM images of EVs derived from *Escherichia coli* cells and watermelon. Scale bar, 100 nm. (B−D) Confocal images and flow cytometric assay of MDA-MB-231 cells incubated with EV-SNA derived from *E. coli* cells. (F−H) Confocal images and flow cytometric assay of MDA-MB-231 cells incubated with EV-SNA derived from watermelon. Both EVs were stained with red membrane dye. Cell nuclei were stained with Hochst33342. Scale bar, 20 μm. Data were represented as mean ± SD (n = 5). ***p < 0.001, by Student's t test.

neously present, the monodisperse EV-SNA assembled into a polymeric form (Figure 2C). DLS measurements demonstrated a significant increase in particle size, further confirming this observation (Figure S5). Taken together, these results demonstrate the successful construction of a DNA-programmed AND logic gate for the controlled manipulation of EV-SNA. The EV-SNA nanostructure introduces a precisely defined and programmable nucleic acid shell to the complex and heterogeneous biological interface of natural EVs, thereby providing unparalleled manipulation of EVs.

2.3. Structure-dependent Efficient Cellular Delivery of EV-SNA

The most important property of SNA nanostructures is their ability to efficiently enter cells without the need for additional transfection reagents.[31] To determine whether EV-SNA exhibits this behavior, we labeled EVs with the lipophilic red fluorescent dye and incubated MDA-MB-231 cells with EV-SNA for 3 h. Both confocal images and flow cytometry showed that the fluorescence signal intensity of cells incubated with EV-SNA was significantly higher than that of cells incubated with native EVs (≈17.6-fold higher EV fluorescence level) (Figure 3A,B). EV-SNA had no significant effect on MDA-MB-231 cell viability (Figure S6). In addition, we found that the red fluorescence signal was not only distributed within the cytoplasm but also showed some signal on the cell membrane. To confirm that EV-SNA was delivered into the cells rather than being adsorbed onto the cell surface, we treated the cells (after incubated with EV-SNA) with trypsin to remove any adsorbed EV-SNA. After trypsin treatment, we observed that the membrane fluorescence signal still remained, and there was no change in the overall fluorescence intensity of the cells, indicating the potential occurrence of membrane fusion (Figure S7). Furthermore, in contrast to the low-efficiency cellular uptake inherent in natural EVs,[37] EV-SNA exhibited a faster cellular uptake dynamic feature (Figure 3C).

Next, we explored the route of uptake of EV-SNA by applying different inhibiting conditions. MDA-MB-231 were pretreated with chlorpromazine (CPZ, a clathrin-dependent endocytosis inhibitor) or methyl-β-cyclodextrin (MβCD, a vesicle-dependent endocytosis inhibitor) and then incubated with EV-SNA, and the fluorescence levels of EV-SNA in cells decreased by approximately 64 or 75%, respectively, compared to the untreated group (Figure S8). Nevertheless, despite such inhibitory effects, the uptake efficiency of the EV-SNA group remained superior to that of the natural EV group without the inhibitor, suggesting that the cellular internalization of EV-SNA is in a large fraction dependent on pathways (e.g., via membrane fusion) other than the above ones. Next, we incubated EV-SNA with cells at 4 °C and found that the fluorescence in the cells was significantly lower than that in the control group, indicating that the cellular uptake of EV-SNA was energy-dependent (Figure S8). These results suggest that EV-SNA enters cells through multiple pathways, including clathrin and caveolin-mediated endocytosis and cell membrane fusion.

To validate the universality of EV-SNA for efficient cell delivery, we investigated the ability of EV-SNA to enter various cell types. We constructed EV-SNA using EVs derived from MDA-MB-231 cells and then coincubated them with MCF-7 (human breast cancer cell line), K150 (human esophageal squamous cancer cell line), HEK293 (human embryonic kidney cell line), NIH-3T3 (mouse embryo fibroblast cell line), and OSRC-2 (human renal carcinoma cell lines) cells, respectively. Both confocal imaging and flow cytometry demonstrated that EV-SNA exhibited significantly enhanced delivery capability, approximately 5−10 times higher compared to native EVs after 3 h incubation (Figure 3D−F).

Having confirmed the efficient entry of EV-SNA into cells, we next investigated the impact of the nucleic acid properties on their efficient cellular entry. We first investigated the impact of DNA density on the entry of EV-SNA into cells. We constructed a series of EV-SNAs with different DNA densities and found that the efficiency of EV-SNA entry into cells increased with the

https://doi.org/10.1021/jacsau.4c00338
JACS Au 2024, 4, 2381−2392

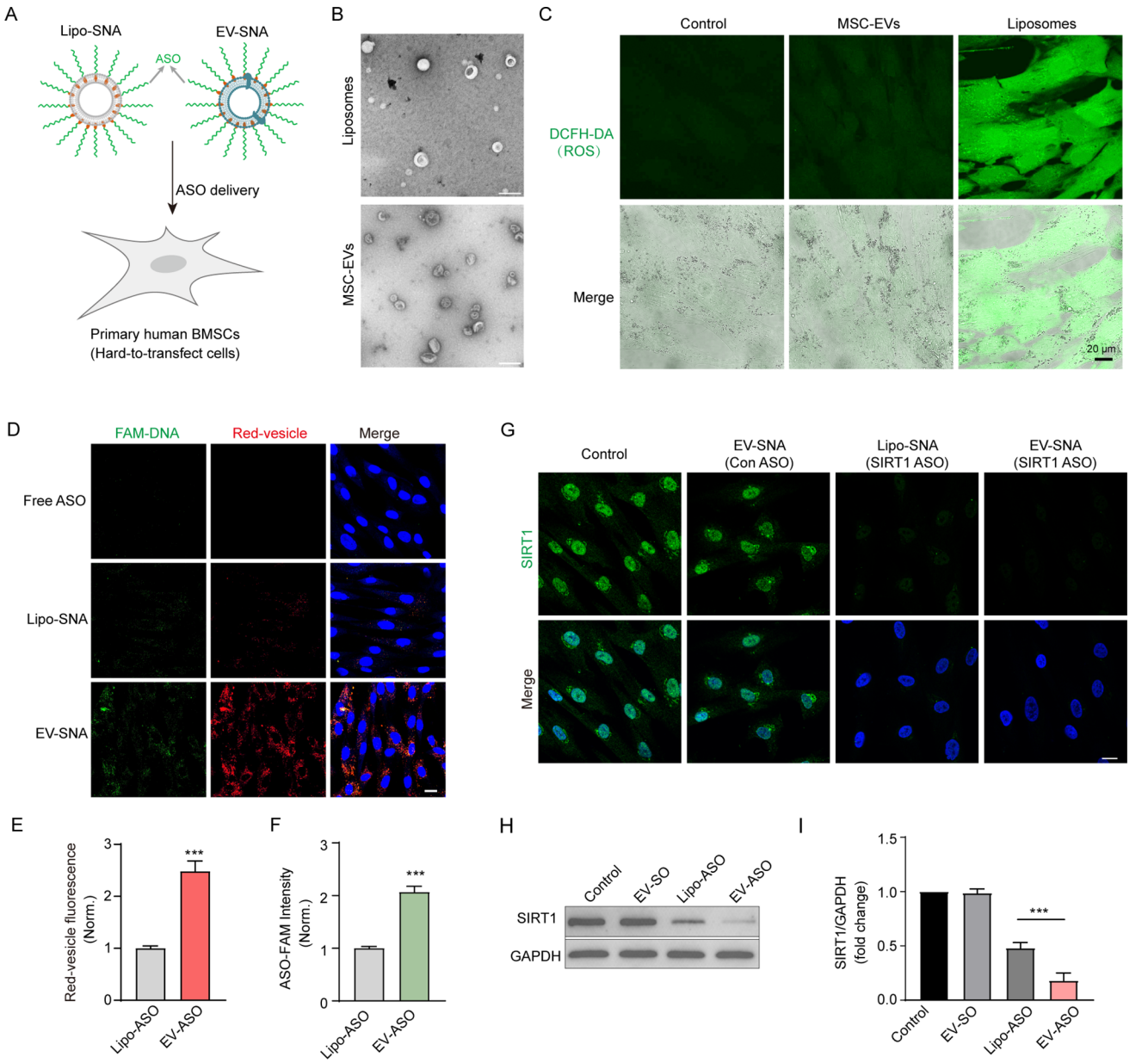

Figure 5. EV-SNA delivers ASOs to modulate protein expression in hard-to-transfect primary human MSCs. (A) Schematic representation of the delivery of ASOs to hard-to-transfuse human MSCs using SNAs with different cores. (B) TEM images of liposomes and EVs derived from human MSCs, respectively. Scale bar, 100 nm. (C) ROS level of human MSCs treated with liposomes and MSC-derived EVs after 12 h. (D) Confocal images of primary human MSCs incubated with endogenous EV-SNAs or liposome-SNA for 3 h. ASO was labeled with FAM. MSC-derived EVs and liposomes were stained with red membrane dye. Scale bar, 20 μm. (E, F) Quantification of the red and green fluorescence levels in MSC cells. Data were represented as mean ± SD ***$p < 0.001$, by Student's t test. (G) MSCs were treated with EV-SNA and liposome-SNA for 6 h, and then cells were cultured with a complete medium for 24 h, after which immunofluorescence of SIRT1 (green) was performed. Scale bar, 20 μm. (H, I) Levels of SIRT1 in MSCs were detected by western blotting. The sense oligonucleotide (SO) was used as the control sense. Data were represented as mean ± SD ***$p < 0.001$, by one-way ANOVA.

DNA surface density. EV-SNAs constructed based on a 1 μM chol-DNA reaction showed a significant enhancement in cellular delivery compared to native EVs (Figure S9). Additionally, compared to the 10 μM group, EV-SNAs constructed based on a 15 μM chol-DNA reaction did not show any further enhancement of cell delivery, indicating that reaching a certain threshold of DNA density does not further promote the cellular delivery of EV-SNA (Figure S9). Thus, the 10 μM concentration of the chol-DNA was chosen for the study hereafter if not otherwise noted.

Next, we investigated the impact of different DNA sequences on the cellular delivery of EV-SNA. We first prepared EV-SNAs composed of different nucleobase types (A, T, C, or G) by adding the same concentration of chol- DNA (14 nt long, 10 μM) into EVs. Then, we assessed the uptake efficiency of various nucleobase types of EV-SNA in various cell types. Flow cytometry analysis and statistical results revealed that all varieties of EV-SNA demonstrated a noticeable enhancement in cellular uptake after 3 h of incubation in multiple cell lines (Figure 3G). Notably, the poly-A group exhibited the highest fluorescence signal intensity, which was significantly 3−4 times

https://doi.org/10.1021/jacsau.4c00338
JACS Au 2024, 4, 2381−2392

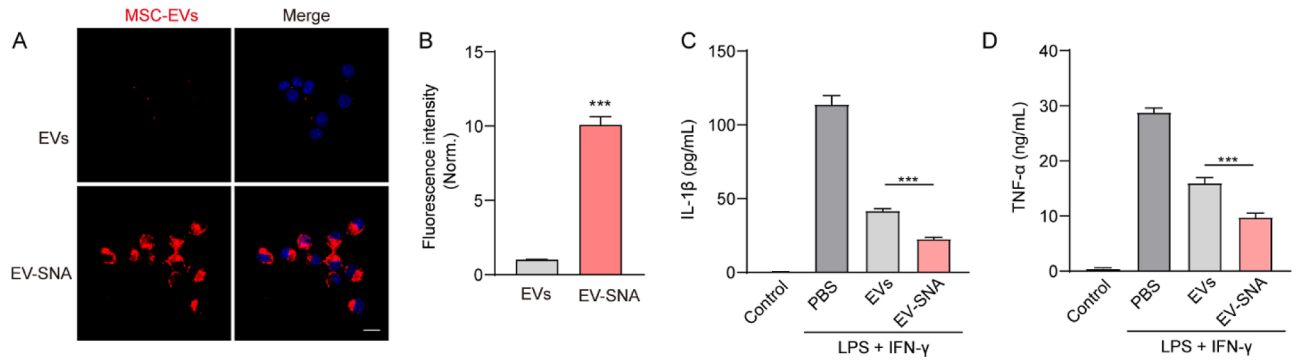

Figure 6. EV-SNA delivery of MSC-EVs regulates inflammatory cytokine production in RAW264.7 cells. (A, B) Confocal images and fluorescence quantification of RAW264.7 cells incubated with MSC-derived EVs or EV-SNA after 3 h. MSC-EVs were stained with red membrane dye. Data were represented as mean ± SEM (n = 5). ***p < 0.001, by Student's t test. Scale bar, 20 μm. (C, D) ELISA results of interleukin-1β (IL-1β) and tumor necrosis factor-α (TNF-α) in the cell culture supernatant. Data were represented as mean ± SD ***p < 0.001, one-way ANOVA.

higher than the other nucleobase-type EV-SNA groups in the three cell types tested (Figures 3G and S10A). The distinct differences in cellular delivery may be attributed to the varying hydrophobicity of these nucleobases. Compared to T, C, and G, poly A is more hydrophobic and enhances the interaction with the cell membrane to improve uptake.[38−40]

Then, we investigated the impact of DNA lengths on the cellular delivery of EV-SNA. We prepared EV-SNAs composed of poly A of different nucleobase lengths (7, 14, 21, and 28 nt) based on MDA-MB-231-derived EVs. The flow cytometry data showed that the fluorescence level of EV-SNA constructed from 7 nt gradually increased in cells compared to native EVs (Figure 3H). Interestingly, as the surface poly A of EV-SNA was prolonged, the fluorescence intensity of the 28 nt group decreased compared with the 21 nt group (Figure S10B).

2.4. EV-SNA Constructed Based on Various Endogenous EVs

Having established the EV-SNA configuration, we next demonstrated the scalability of the endogenous EV core. Almost all living organisms have been found to release nanoscale EVs.[41,42] We extracted EVs from the cells of a plant (watermelon) and a bacterial (*E. coli*), respectively, according to previously described methods.[43,44] Cryo-EM images revealed that EVs derived from *E. coli* and watermelon exhibited typical vesicular structures, with sizes smaller than 100 nm (Figure 4A,E). These EVs were separately vortexed with chol-DNA (10 μM) ligands at room temperature for 5 min to construct EV-SNA. Following incubation with chol-DNA, a marked increase in hydrated particle size and a significant decrease in zeta potential were observed (Figure S11), indicating the successful construction of SNA nanostructures from EVs of various species origins.

Next, we investigated the internalization of these EV-SNA by the human cell line. In the native EV groups, only a few fluorescence signals was observed, whereas when deployed with chol-DNA, all EV-SNA groups showed intense EV fluorescence signals distributed in the cytoplasm (Figure 4B,F). Flow cytometry data revealed prominently increased cellular fluorescence intensities resulting from the EV-SNA (≈10.7, and 9.5 folds of increase for EV-SNA from *E. coli*, and watermelon, respectively) relative to those native EVs (Figure 4C,D,G,H). These results confirm that EV-SNAs with efficient cell delivery can be constructed based on a variety of endogenous EVs.

2.5. EV-SNA Delivery of Functional Nucleic Acids and EVs

As a proof of concept, we finally demonstrate that EV-SNA can be utilized for delivering functional EVs or exogenous nucleic acids.

First, we demonstrated that EV-SNA constructed based on natural EVs exhibits better cell compatibility and nucleic acid delivery capability compared to liposome-based cores. The majority of studies on cell delivery utilize model cell lines as the experimental subjects, rather than cells relevant to the intended applications, thereby diminishing the usefulness of the research. Specifically, "hard-to-transfect cells," such as immune cells, nerve cells, and stem cells, are a group of cell types crucial for various technologies, which are notably challenging in terms of delivering exogenous entities intracellularly.[45] Hence, we opted to assess the delivery efficiency of EV-SNA using primary human mesenchymal stem cells (MSCs) as representatives of "hard-to-transfect cells" (Figure 5A). MSC-derived EVs and artificial liposomes share similar vesicle structures and nanoscale sizes (Figures 5B and S12). We first evaluated the impact of MSC-EVs and liposomes on primary MSCs. Both EVs and liposomes had no significant effect on the cell number of hMSCs (Figure S13A). However, we observed a significant increase in intracellular ROS fluorescence levels in the liposome-treated group, while the MSC-EV group showed no significant change compared to the control group, indicating the excellent biocompatibility of endogenous EVs (Figure 5C).

To validate whether EV-SNA can effectively deliver nucleic acids into primary human MSCs, we constructed endogenous EV-SNA and Lipo-SNA with ASOs as the shells (Figure 5A). NAD-dependent protein deacetylase sirtuin-1 (SIRT1) was selected as the target protein for study.[46] The FAM-labeled ASO was inserted into the phospholipid bilayer of EVs or liposomes (both labeled with lipophilic red fluorescent dye) through hydrophobic interactions to form the SNA nanostructure. After coincubation with MSCs for 3 h, confocal imaging revealed that both red and green fluorescence signals of MSCs in the EV-SNA group were significantly higher (≈2.5-fold) than those in the Lipo-SNA group. No significant fluorescence signal was observed in the free ASO group (Figure 5D−F). These results suggest that the delivery efficiency of EV-SNA constructed from homologous EVs is significantly better than that of Lipo-SNA in hard-to-transfect MSC cells, which may be related to the biological characteristics of EVs. Next, we subjected primary MSCs to anti-SIRT1 EV-SNA, anti-SIRT1 Lipo-SNA, and control sense EV-SNA with a SO. The knockdown levels of the

https://doi.org/10.1021/jacsau.4c00338
JACS Au 2024, 4, 2381−2392

SIRT1 protein were assessed through immunofluorescence and Western blot analysis. Immunofluorescence images showed that anti-SIRT1 EV-SNA and anti-SIRT1 Lipo-SNA both successfully knocked down the expression of SIRT1 in MSCs. However, the intracellular green fluorescence signal of SIRT1 in the EV-SNA group was reduced by approximately 36% compared to the Lipo-SNA group (Figures 5G and S14). Western blot results showed that the grayscale value of SIRT1 in the anti-SIRT1 EV-SNA group decreased by approximately 2.7 times compared to the Lipo-ASO group, further confirming the enhanced ASO delivery and protein expression knockdown capability of EV-SNA (Figure 5H,I). Taken together, these findings indicate that EV-SNA constructed through endogenous EVs exhibits superior biocompatibility and enhanced delivery efficiency compared to liposomes in hard-to-transfect MSC cells.

Next, we assessed the therapeutic potential of EV-SNA configurations to improve the delivery of functional EVs. MSC-derived EVs can encapsulate functional contents, offering great promise as a feasible and effective biological treatment for inflammation-related diseases.[47] Enhancing the delivery efficiency of MSC-EVs will further advance their potential as a promising cell-free immunoregulatory therapeutic agent.[48] We extracted EVs from the primary human MSC medium and constructed EV-SNA, according to previously described methods. To evaluate the anti-inflammatory effects of EV-SNA, we established an LPS and IFN-γ costimulated and induced RAW264.7 cell (a macrophage cell line) polarization model. RAW264.7 cells were cocultured with lipophilic red fluorescent dye-labeled EV-SNA or MSC-EVs. Remarkably, the EV-SNA group was significantly more intense (≈10-fold higher EV fluorescence level) than native MSC-EVs after a short 3 h incubation (Figure 6A,B). Next, RAW264.7 cells were pretreated with EVs or EV-SNA for 3 h and then stimulated with LPS and IFN-γ for 12 h. The release of pro-inflammatory factors TNF-α and IL-1β were significantly upregulated in the LPS- and IFN-γ-costimulated group compared to untreated cells. Of note, compared to native MSC-EV treatment, we observed a more pronounced inhibitory effect on the release of TNF-α and IL-1β with EV-SNA treatment (Figure 6C,D). Taken together, EV-SNA can be used to efficiently deliver functional EVs.

3. CONCLUSIONS

In summary, we have developed a class of EV-SNAs. This architecture can be rapidly and easily assembled from widely available and easily obtained natural EVs. This system shows several advantages:

(1) Highly modular: the construction of EV-SNA relies on the insertion of hydrophobic groups into the phospholipid bilayer and the fundamental structure of all types of EVs, while the delivery properties of EV-SNA primarily depend on the 3D stretched nucleic acid structure. Consequently, EV-SNA components are highly modular and replaceable, enabling the construction of a diverse library of natural EV cores and nucleic acid shells for EV-SNA applications under varying requirements.

(2) Efficient cellular delivery: EV-SNA has demonstrated unparalleled rapid and efficient cellular delivery capabilities, exhibiting superior delivery characteristics over liposomes in hard-to-transfect cells. This advancement establishes a robust therapeutic platform for the future delivery of a wide range of endogenous or exogenous cargoes utilizing EV-SNA.

(3) Flexible scalability: the programmable nucleic acid shell on the surface of EV-SNA provides it with a designable manipulability and flexible expandability. In theory, various functional groups or drug molecules can be loaded onto the surface of EV-SNA based on base pairing complementarity or encapsulated within vesicular lumen for efficient delivery.

Taken together, the EV-SNA, as a novel material form, provides a new framework paradigm for EV-based applications in drug delivery, disease treatment, nanovaccines, and other fields.

4. METHODS

4.1. DNA Oligonucleotides

All DNA oligonucleotides were synthesized and purchased from Sangon Biological Engineering Technology & Co. Ltd. (Shanghai, China) and purified by HPLC. All DNA strands were dissolved in PBS.

4.2. Cell Culture

MDA-MB-231, NIH3T3, HEK293, and RAW264.7 cells were cultured in Dulbecco's modified Eagle medium (DMEM) (Gibco, 11965118) containing 10% heat-inactivated fetal bovine serum (FBS) (Gibco, 10099141C), 2 mM L-glutamine (Beyotime, C0212), and 1% penicillin/streptomycin (Beyotime, C0222). KYSE-150 and OS-RC-2 cells were cultured in Roswell Park Memorial Institute 1640 (RPMI 1640) (Gibco, 11875093) medium containing 10% FBS, 2 mM 100× L-glutamine, and 1% penicillin/streptomycin. Primary human umbilical cord MSCs were cultured in Dulbecco's modified Eagle medium/nutrient mixture F-12 (DMEM/F-12) (Gibco, 21331020) medium containing 10% FBS, 2 mM 100X L-glutamine, and 1% penicillin/streptomycin at 37 °C in humidified conditions equilibrated with 5% CO_2.

4.3. EV Isolation

An ultracentrifugation procedure was used to isolate and concentrate EVs. Briefly, when the cells reached 80% confluence, the culture medium was completely discarded and washed three times with PBS. The fresh serum-free medium was then added to the cells for 24 h. The cell culture medium was centrifuged at 300g for 10 min and 3000g for 20 min to remove the cells and cell fragments at 4 °C. For each centrifugation, only the supernatant was saved, discarding the precipitate produced by the centrifugation. The supernatant was centrifuged at 10,000g for 30 min and then filtered through a 0.22 μm filter. The EVs were then collected by centrifugation at 100,000g for 90 min at 4 °C using a CP100NX ultracentrifuge (Hitachi, Japan) with a P28S2 horizontal rotor (Hitachi, Japan). EVs were resuspended in 500 μL PBS and stored at −80 °C for further analysis. EV yields were determined using the BCA protein kit according to the manufacturer's instructions.

To isolate *E. coli*-derived EVs, 50 mL LB (Luria−Bertani) liquid medium was centrifuged twice at 10,000g for 30 min and filtered twice through 0.22 μm filters. *E. coli*-derived EVs were collected by ultracentrifugation at 100,000g for 120 min at 4 °C. Finally, the EVs were resuspended in 500 μL PBS and stored at −80 °C for further analysis.

To isolate watermelon EVs, watermelon juice was extracted by physical squeezing. The watermelon juice was diluted 1:3 with PBS and then centrifuged at 1000g for 10 min and then twice at 3000g for 20 min. The supernatant was centrifuged twice at 10,000g for 30 min and filtered through a 0.22 μm filter. Watermelon EVs were collected by ultracentrifugation at 100,000g for 120 min at 4 °C. The EVs were resuspended in PBS and stored at −80 °C for further analysis.

Sizes and concentrations of EVs were obtained using a Nano Sight NS300 system (Malvern, the United Kingdom).

4.4. SNA Construction

EVs (3 μg, 60 μL) were gently vortexed (500 rpm, Vortex-5 Vortex Mixer) with the chol-DNA (i.e., cholesterol-DNA, 10 μM) for 5 min at

https://doi.org/10.1021/jacsau.4c00338
JACS Au 2024, 4, 2381−2392

room temperature. Samples were washed three times with PBS buffer through 100k MWCO filters (Millipore Sigma) at 5000*g* for 5 min to remove excess oligonucleotides. For Lipo-SNA construction, liposomes (Avanti, 300205S) were gently vortexed with the chol-DNA (10 μM) for 5 min and then washed three times with PBS buffer through 100k MWCO filters (Millipore Sigma) at 5000*g* for 5 min to remove excess oligonucleotides.

The hydrodynamic size and zeta potential were performed on a Litesizer 500 (Anton Paar, Austrian). All experiments were performed at 25 °C.

To observe the colocalization of EVs and chol-DNA, EVs derived from MDA-MB-231 cells were labeled with red ExoSparkler dye and modified with FAM-Chol-DNA. The EV-SNA medium was diluted with PBS (1:100) and then adsorbed onto poly-D-lysine-coated glass bottom plates. Fluorescence images of EV-SNA were obtained using total internal reflection fluorescence microscopy (TIRFM, Leica).

For TEM imaging, 10 μL of EV solution was pipetted onto a copper grid and incubated for 15 min, and then, the copper grid was drained along the edges with a filter paper. Negative staining was performed by incubating the copper grid with 10 μL of 1% uranyl acetate for 90 s and removing excess liquid with a filter paper. The TEM images were obtained with a Hitachi HT7800 high-contrast transmission electron microscope (Hitachi, Japan). Cryo-EM images of EVs were obtained using a transmission electron microscope system (Talos F200C G2).

4.5. Amount of DNA on EV-SNA

To estimate the loading of DNA ligands on EVs, 3′-FAM-labeled DNA ligands were used to modify EVs by vortexing (500 rpm, 5 min). The product was divided into two fractions. One fraction was measured with a NanoSight NS300 system (Malvern), generating the EV particle molar concentration. The other fraction was cleaved by 5% Triton-100 for 5 min, and then, the fluorescence intensity was read (Ex. 494/Em. 520) with a microplate reader (BioTek, Synergy H4). The molar concentration of the FAM-DNA ligands was estimated by plotting the measured fluorescence intensity on the calibration curve generated with those of known concentrations. The final number of DNA deployed on EVs was calculated by dividing the molar concentration of DNA ligands by the number of EVs.

4.6. Gel Electrophoresis Analysis

Equal molar amounts of S1 (5 μM), S2 (5 μM), and aptamer (5 μM) were mixed and then annealed at 90 °C for 10 min, followed by slow cooling to room temperature before use. Then, the abovementioned system was incubated with or without Linker (5 μM) and ATP (2 mM) for 3 h at 37 °C. Characterization was carried out using 10% polyacrylamide gel electrophoresis. Gels were electrophoresed at 100 V for 4 h and stained with Gelred, and electrophoretic images were obtained on a Bio-Rad imager (ChemiDoc MP, China).

4.7. DNA-Induced Logic-Gated Assembly of EVs

Equimolar amounts of A-chol (80 μM) and ATP aptamer (80 μM) were mixed, annealed at 90 °C for 10 min, and slowly cooled to room temperature to form the apt-A-chol complex. Subsequently, EVs (3 μg, 60 μL) were mixed with apt-A-chol (40 μM, 20 μL) and B-chol (40 μM, 20 μL), respectively, by slow spinning (500 rpm, Vortex-5 Vortex Mixer) for 5 min at room temperature. All samples were buffered with PBS buffer through a 100k MWCO filter (Millipore Sigma) at 5000*g* for 5 min to remove excess nucleotides. EV-SNAs constructed with different DNA strand modifications as described above were mixed, and then, the system was incubated with or without C-linker (5 μM) and ATP (2 mM) for 3 h at 37 °C. All samples were examined by TEM.

4.8. Cellular Internalization of EV-SNA

Before cellular internalization, EVs were labeled with ExoSparkler Exosome Membrane Labeling Kit-red (Dojindo, EX02) according to the manufacturer's protocols. Cells were seeded at a density of 10,000 cells/well in 14 mm glass bottom plates (Cellvis, D29-14-1-N) and cultured for 48 h. The medium was then completely discarded and washed three times with PBS to remove the residual medium. After incubation with 3.0 μg EVs or EV-SNA in serum-free media for 3 h at 37 °C, the cells were washed three times and fixed in 4% paraformaldehyde solution. Cell membranes were labeled with PlasMem Bright Green (Dojindo, P504), and cell nuclei were stained with Hoechst 33342 (Dojindo, H342). The fluorescence images were acquired using a Leica TCS SP8 confocal fluorescence microscope (Leica, Germany), and fluorescence intensity was analyzed using LAS AF Lite software.

For flow cytometric analysis, 200 μL suspended cells (1×10^6 cells/mL) were treated with 3 μg EVs or EV-SNA for 3 h at 37 °C and then analyzed using Becton Dickinson LSR Fortessa flow cytometry (Becton Dickinson, USA). Data were analyzed using FlowJo software.

In the trypsin treatment experiment, 300 μL suspended cells (3×10^5 cells/mL) were incubated with 3 μg EVs or EV-SNA for 3 h at 37 °C in fresh serum-free medium, and then, EV-SNA treatment groups were divided into two parts, one of which was incubated with trypsin (Gibco, 25200072) for 15 min at 37 °C. After incubation, cells were washed three times with cold PBS and fixed with a 4% paraformaldehyde solution.

For the EV internalization inhibition, MDA-MB-231 cells were seeded at a density of 10, 000 cells/well in 14 mm glass-bottom plates (Cellvis, D29-14-1-N) and cultured for 48 h. The medium was then discarded and washed three times with PBS. The cells were pretreated with 5 μM chlorpromazine (Selleck, S5749) or 5 mM methyl β-cyclodextrin (Selleck, S6827) or incubated at 4 °C for 30 min, and then, the 3 μg EVs or EV-SNA were added for further 3 h incubation. The cells were then washed three times. The images were acquired using a confocal fluorescence microscope.

4.9. Stimulation of RAW 264.7 Cells

To induce an inflammatory model, RAW264.7 cells were seeded in a 24-well plate at a density of 2×10^5 cells per well for 24 h. RAW264.7 cells were pretreated with 5 μg EVs or 5 μg EV-SNA for 3 h and then stimulated with lipopolysaccharide (1 μg/mL) (Beyotime, S1732) and recombinant murine IFN-γ (20 ng/mL) (Beyotime, P6137) for 12 h. The resulting supernatant was collected to test the levels of TNF-α and IL-1β using the mouse TNF-α ELISA kit (Jianglaibio Co. Ltd., JL10484) and mouse IL-1β ELISA kit (Abcam, ab197742) according to the manufacturer's instructions.

4.10. Immunofluorescence Analysis

Primary human umbilical cord MSCs were seeded at a density of 10,000 cells/well in 14 mm glass bottom plates for 48 h. The cells were washed three times. 5.0 μg Lipo-SNA or EV-SNA constructed by ASOs derived from the mRNA nucleotide sequence of sirtuin-1 gene (SIRT1-ASO) was incubated in serum-free medium for 6 h at 37 °C, and then, the culture was replaced with complete medium for 24 h. The cells were then fixed with 4% PFA, blocked with 1% BSA (Sigam, V900933), and permeabilized with 0.4% Triton X-100 (Beyotime, ST795). The cells were then incubated with an anti-SIRT1 antibody (Abcam, ab32441) overnight at 4 °C. The cells were then incubated with secondary antibody Alexa Fluor 488 goat antirabbit (Abcam, ab150077) for 1 h at room temperature. The fluorescence images were acquired using a Leica TCS SP8 confocal fluorescence microscope.

4.11. Statistical Analysis

Data analysis was performed with GraphPad Prism 8, and data were presented as mean ± SD from at least three independent experiments unless otherwise stated in the figure legend. The statistical significance of the different groups was evaluated by one-way ANOVA or Student's *t* test. $*p < 0.05$, $**p < 0.01$, $***p < 0.001$, ns means not significant.

■ ASSOCIATED CONTENT

Supporting Information

The Supporting Information is available free of charge at https://pubs.acs.org/doi/10.1021/jacsau.4c00338.

DNA sequences, additional characterization of EVs and EV-SNA of different biological origins, cell delivery of EV-SNA, mechanism of EV-SNA uptake, and EVS-SNA cytotoxicity in this study (PDF)

https://doi.org/10.1021/jacsau.4c00338
JACS Au 2024, 4, 2381−2392

AUTHOR INFORMATION

Corresponding Authors

Jiang Li − *Institute of Materiobiology, Department of Chemistry, College of Science, Shanghai University, Shanghai 200444, China*; Email: lijiang80@shu.edu.cn

Kaizhe Wang − *Ningbo Key Laboratory of Biomedical Imaging Probe Materials and Technology, Ningbo Cixi Institute of Biomedical Engineering, Ningbo Institute of Materials Technology and Engineering, Chinese Academy of Sciences, Ningbo 315300, China; University of Chinese Academy of Sciences, Beijing 100049, China;* orcid.org/0000-0003-0331-6847; Email: wangkaizhe@nimte.ac.cn

Jianping Zheng − *Ningbo Key Laboratory of Biomedical Imaging Probe Materials and Technology, Ningbo Cixi Institute of Biomedical Engineering, Ningbo Institute of Materials Technology and Engineering, Chinese Academy of Sciences, Ningbo 315300, China; University of Chinese Academy of Sciences, Beijing 100049, China;* orcid.org/0000-0001-6014-5197; Email: zhengjianping@nimte.ac.cn

Authors

Hao Chen − *Ningbo Key Laboratory of Biomedical Imaging Probe Materials and Technology, Ningbo Cixi Institute of Biomedical Engineering, Ningbo Institute of Materials Technology and Engineering, Chinese Academy of Sciences, Ningbo 315300, China; University of Chinese Academy of Sciences, Beijing 100049, China*

Qiaojiao Ding − *Cixi Biomedical Research Institute, Wenzhou Medical University, Wenzhou 325035, China*

Lin Li − *Ningbo Key Laboratory of Biomedical Imaging Probe Materials and Technology, Ningbo Cixi Institute of Biomedical Engineering, Ningbo Institute of Materials Technology and Engineering, Chinese Academy of Sciences, Ningbo 315300, China*

Pengyao Wei − *Cixi Biomedical Research Institute, Wenzhou Medical University, Wenzhou 325035, China*

Zitong Niu − *Cixi Biomedical Research Institute, Wenzhou Medical University, Wenzhou 325035, China*

Tong Kong − *Ningbo Key Laboratory of Biomedical Imaging Probe Materials and Technology, Ningbo Cixi Institute of Biomedical Engineering, Ningbo Institute of Materials Technology and Engineering, Chinese Academy of Sciences, Ningbo 315300, China*

Pan Fu − *Ningbo Key Laboratory of Biomedical Imaging Probe Materials and Technology, Ningbo Cixi Institute of Biomedical Engineering, Ningbo Institute of Materials Technology and Engineering, Chinese Academy of Sciences, Ningbo 315300, China*

Yuhui Wang − *Ningbo Key Laboratory of Biomedical Imaging Probe Materials and Technology, Ningbo Cixi Institute of Biomedical Engineering, Ningbo Institute of Materials Technology and Engineering, Chinese Academy of Sciences, Ningbo 315300, China; University of Chinese Academy of Sciences, Beijing 100049, China;* orcid.org/0000-0001-9430-6614

Complete contact information is available at: https://pubs.acs.org/10.1021/jacsau.4c00338

Author Contributions

[⊥]H.C. and Q.D. contributed equally to this work.

Notes

The authors declare no competing financial interest.

ACKNOWLEDGMENTS

H.C. and Q.D. contributed equally to this work. This work was supported by the National Natural Science Foundation of China (nos. 22105124 and 22325406), the Ningbo Yongjiang Talent Introduction Programme (no. 2023A-114-G), the "Science and Innovation Yongjiang 2035" Key R&D Programme of Ningbo, the Chunlei Foundation of Ningbo Institute of Materials Technology and Engineering (NIMTE), CAS, the foundation of the director of Ningbo Institute of Materials Technology and Engineering (NIMTE), CAS (no. 2021SZKY0203), and the Natural Science Foundation of Ningbo City (no. 2022J046).

REFERENCES

(1) Raposo, G.; Stahl, P. D. Extracellular vesicles: a new communication paradigm? *Nat. Rev. Mol. Cell Biol.* **2019**, *20* (9), 509−510.

(2) Armstrong, J. P.; Holme, M. N.; Stevens, M. M. Re-Engineering Extracellular Vesicles as Smart Nanoscale Therapeutics. *ACS Nano* **2017**, *11* (1), 69−83.

(3) Tenchov, R.; Sasso, J. M.; Wang, X.; Liaw, W.-S.; Chen, C.-A.; Zhou, Q. A. Exosomes−Nature's Lipid Nanoparticles, a Rising Star in Drug Delivery and Diagnostics. *ACS Nano* **2022**, *16* (11), 17802−17846.

(4) Wang, K.; Wei, Y.; Xie, X.; Li, Q.; Liu, X.; Wang, L.; Li, J.; Wu, J.; Fan, C. DNA-Programmed Stem Cell Niches via Orthogonal Extracellular Vesicle-Cell Communications. *Adv. Mater.* **2023**, *35* (45), 2302323.

(5) You, Y.; Tian, Y.; Yang, Z.; Shi, J.; Kwak, K. J.; Tong, Y.; Estania, A. P.; Cao, J.; Hsu, W. H.; Liu, Y.; Chiang, C. L.; Schrank, B. R.; Huntoon, K.; Lee, D.; Li, Z.; Zhao, Y.; Zhang, H.; Gallup, T. D.; Ha, J.; Dong, S.; Li, X.; Wang, Y.; Lu, W. J.; Bahrani, E.; Lee, L. J.; Teng, L.; Jiang, W.; Lan, F.; Kim, B. Y. S.; Lee, A. S. Intradermally delivered mRNA-encapsulating extracellular vesicles for collagen-replacement therapy. *Nat. Biomed. Eng.* **2023**, *7* (7), 887−900.

(6) Liu, M.; Hu, S.; Yan, N.; Popowski, K. D.; Cheng, K. Inhalable extracellular vesicle delivery of IL-12 mRNA to treat lung cancer and promote systemic immunity. *Nat. Nanotechnol.* **2024**, *19* (4), 565−575.

(7) Lathwal, S.; Yerneni, S. S.; Boye, S.; Muza, U. L.; Takahashi, S.; Sugimoto, N.; Lederer, A.; Das, S. R.; Campbell, P. G.; Matyjaszewski, K. Engineering exosome polymer hybrids by atom transfer radical polymerization. *Proc. Natl. Acad. Sci. U.S.A.* **2021**, *118* (2), No. e2020241118.

(8) Kumar, S.; Michael, I. J.; Park, J.; Granick, S.; Cho, Y.-K. Cloaked Exosomes: Biocompatible, Durable, and Degradable Encapsulation. *Small* **2018**, *14* (34), 1802052.

(9) Stranford, D. M.; Simons, L. M.; Berman, K. E.; Cheng, L.; DiBiase, B. N.; Hung, M. E.; Lucks, J. B.; Hultquist, J. F.; Leonard, J. N. Genetically encoding multiple functionalities into extracellular vesicles for the targeted delivery of biologics to T cells. *Nat. Biomed. Eng.* **2023**, *8*, 397−414.

(10) Hade, M. D.; Suire, C. N.; Suo, Z. Significant Enhancement of Fibroblast Migration, Invasion, and Proliferation by Exosomes Loaded with Human Fibroblast Growth Factor 1. *ACS Appl. Mater. Interfaces* **2024**, *16* (2), 1969−1984.

(11) Alvarez-Erviti, L.; Seow, Y.; Yin, H.; Betts, C.; Lakhal, S.; Wood, M. J. Delivery of siRNA to the mouse brain by systemic injection of targeted exosomes. *Nat. Biotechnol.* **2011**, *29* (4), 341−345.

(12) Xie, Y.; Sun, Y.; Liu, Y.; Zhao, J.; Liu, Q.; Xu, J.; Qin, Y.; He, R.; Yuan, F.; Wu, T.; Duan, C.; Jiang, L.; Lu, H.; Hu, J. Targeted Delivery of RGD-CD146(+)CD271(+) Human Umbilical Cord Mesenchymal Stem Cell-Derived Exosomes Promotes Blood-Spinal Cord Barrier Repair after Spinal Cord Injury. *ACS Nano* **2023**, *17* (18), 18008−18024.

(13) Zou, J.; Shi, M.; Liu, X.; Jin, C.; Xing, X.; Qiu, L.; Tan, W. Aptamer-Functionalized Exosomes: Elucidating the Cellular Uptake Mechanism and the Potential for Cancer-Targeted Chemotherapy. *Anal. Chem.* **2019**, *91* (3), 2425−2430.
(14) Zhuang, J.; Tan, J.; Wu, C.; Zhang, J.; Liu, T.; Fan, C.; Li, J.; Zhang, Y. Extracellular vesicles engineered with valency-controlled DNA nanostructures deliver CRISPR/Cas9 system for gene therapy. *Nucleic Acids Res.* **2020**, *48* (16), 8870−8882.
(15) Qi, H.; Liu, C.; Long, L.; Ren, Y.; Zhang, S.; Chang, X.; Qian, X.; Jia, H.; Zhao, J.; Sun, J.; Hou, X.; Yuan, X.; Kang, C. Blood Exosomes Endowed with Magnetic and Targeting Properties for Cancer Therapy. *ACS Nano* **2016**, *10* (3), 3323−3333.
(16) Bhatta, R.; Han, J.; Liu, Y.; Bo, Y.; Lee, D.; Zhou, J.; Wang, Y.; Nelson, E. R.; Chen, Q.; Zhang, X. S.; Hassaneen, W.; Wang, H. Metabolic tagging of extracellular vesicles and development of enhanced extracellular vesicle based cancer vaccines. *Nat. Commun.* **2023**, *14* (1), 8047.
(17) Zheng, W.; Radler, J.; Sork, H.; Niu, Z.; Roudi, S.; Bost, J. P.; Gorgens, A.; Zhao, Y.; Mamand, D. R.; Liang, X.; Wiklander, O. P. B.; Lehto, T.; Gupta, D.; Nordin, J. Z.; El Andaloussi, S. Identification of scaffold proteins for improved endogenous engineering of extracellular vesicles. *Nat. Commun.* **2023**, *14* (1), 4734.
(18) Zhang, H.; Freitas, D.; Kim, H. S.; Fabijanic, K.; Li, Z.; Chen, H.; Mark, M. T.; Molina, H.; Martin, A. B.; Bojmar, L.; Fang, J.; Rampersaud, S.; Hoshino, A.; Matei, I.; Kenific, C. M.; Nakajima, M.; Mutvei, A. P.; Sansone, P.; Buehring, W.; Wang, H.; Jimenez, J. P.; Cohen-Gould, L.; Paknejad, N.; Brendel, M.; Manova-Todorova, K.; Magalhaes, A.; Ferreira, J. A.; Osorio, H.; Silva, A. M.; Massey, A.; Cubillos-Ruiz, J. R.; Galletti, G.; Giannakakou, P.; Cuervo, A. M.; Blenis, J.; Schwartz, R.; Brady, M. S.; Peinado, H.; Bromberg, J.; Matsui, H.; Reis, C. A.; Lyden, D. Identification of distinct nanoparticles and subsets of extracellular vesicles by asymmetric flow field-flow fractionation. *Nat. Cell Biol.* **2018**, *20* (3), 332−343.
(19) Kowal, J.; Arras, G.; Colombo, M.; Jouve, M.; Morath, J. P.; Primdal-Bengtson, B.; Dingli, F.; Loew, D.; Tkach, M.; Thery, C. Proteomic comparison defines novel markers to characterize heterogeneous populations of extracellular vesicle subtypes. *Proc. Natl. Acad. Sci. U.S.A.* **2016**, *113* (8), E968−E977.
(20) Mirkin, C. A.; Letsinger, R. L.; Mucic, R. C.; Storhoff, J. J. A DNA-based method for rationally assembling nanoparticles into macroscopic materials. *Nature* **1996**, *382* (6592), 607−609.
(21) Cutler, J. I.; Auyeung, E.; Mirkin, C. A. Spherical nucleic acids. *J. Am. Chem. Soc.* **2012**, *134* (3), 1376−1391.
(22) Rosi, N. L.; Giljohann, D. A.; Thaxton, C. S.; Lytton-Jean, A. K.; Han, M. S.; Mirkin, C. A. Oligonucleotide-modified gold nanoparticles for intracellular gene regulation. *Science* **2006**, *312* (5776), 1027−1030.
(23) Fang, Y.; Lu, X.; Wang, D.; Cai, J.; Wang, Y.; Chen, P.; Ren, M.; Lu, H.; Union, J.; Zhang, L.; Sun, Y.; Jia, F.; Kang, X.; Tan, X.; Zhang, K. Spherical Nucleic Acids for Topical Treatment of Hyperpigmentation. *J. Am. Chem. Soc.* **2021**, *143* (3), 1296−1300.
(24) Jiao, K.; Yan, Q.; Guo, L.; Qu, Z.; Cao, S.; Chen, X.; Li, Q.; Zhu, Y.; Li, J.; Wang, L.; Fan, C.; Wang, F. Poly-Adenine-Based Spherical Nucleic Acids for Efficient Live-Cell MicroRNA Capture. *Angew. Chem., Int. Ed. Engl.* **2021**, *60* (26), 14438−14445.
(25) Li, H.; Zhang, B.; Lu, X.; Tan, X.; Jia, F.; Xiao, Y.; Cheng, Z.; Li, Y.; Silva, D. O.; Schrekker, H. S.; Zhang, K.; Mirkin, C. A. Molecular spherical nucleic acids. *Proc. Natl. Acad. Sci. U.S.A.* **2018**, *115* (17), 4340−4344.
(26) Vasher, M. K.; Yamankurt, G.; Mirkin, C. A. Hairpin-like siRNA-Based Spherical Nucleic Acids. *J. Am. Chem. Soc.* **2022**, *144* (7), 3174−3181.
(27) Zhu, S.; Xing, H.; Gordiichuk, P.; Park, J.; Mirkin, C. A. PLGA Spherical Nucleic Acids. *Adv. Mater.* **2018**, *30* (22), No. e1707113.
(28) Banga, R. J.; Chernyak, N.; Narayan, S. P.; Nguyen, S. T.; Mirkin, C. A. Liposomal spherical nucleic acids. *J. Am. Chem. Soc.* **2014**, *136* (28), 9866−9869.
(29) Callmann, C. E.; Cole, L. E.; Kusmierz, C. D.; Huang, Z.; Horiuchi, D.; Mirkin, C. A. Tumor cell lysate-loaded immunostimulatory spherical nucleic acids as therapeutics for triple-negative breast cancer. *Proc. Natl. Acad. Sci. U.S.A.* **2020**, *117* (30), 17543−17550.
(30) Brodin, J. D.; Sprangers, A. J.; McMillan, J. R.; Mirkin, C. A. DNA-Mediated Cellular Delivery of Functional Enzymes. *J. Am. Chem. Soc.* **2015**, *137* (47), 14838−14841.
(31) Huang, C.; Han, Z.; Evangelopoulos, M.; Mirkin, C. A. CRISPR Spherical Nucleic Acids. *J. Am. Chem. Soc.* **2022**, *144* (41), 18756−18760.
(32) Johnsen, K. B.; Gudbergsson, J. M.; Duroux, M.; Moos, T.; Andresen, T. L.; Simonsen, J. B. On the use of liposome controls in studies investigating the clinical potential of extracellular vesicle-based drug delivery systems - A commentary. *J. Controlled Release* **2018**, *269*, 10−14.
(33) Gelibter, S.; Marostica, G.; Mandelli, A.; Siciliani, S.; Podini, P.; Finardi, A.; Furlan, R. The impact of storage on extracellular vesicles: A systematic study. *J. Extracell. Vesicles* **2022**, *11* (2), No. e12162.
(34) Chen, Y.; Chen, X.; Zhang, B.; Zhang, Y.; Li, S.; Liu, Z.; Gao, Y.; Zhao, Y.; Yan, L.; Li, Y.; Tian, T.; Lin, Y. DNA framework signal amplification platform-based high-throughput systemic immune monitoring. *Signal Transduction Targeted Ther.* **2024**, *9* (1), 28.
(35) Li, Y.; Cai, Z.; Ma, W.; Bai, L.; Luo, E.; Lin, Y. A DNA tetrahedron-based ferroptosis-suppressing nanoparticle: superior delivery of curcumin and alleviation of diabetic osteoporosis. *Bone Res.* **2024**, *12* (1), 14.
(36) Bai, L.; Feng, M.; Zhang, Q.; Cai, Z.; Li, Q.; Li, Y.; Ma, C.; Xiao, J.; Lin, Y. Synergistic Osteogenic and Antiapoptotic Framework Nucleic Acid Complexes Prevent Diabetic Osteoporosis. *Adv. Funct. Mater.* **2024**, 2314789.
(37) Bonsergent, E.; Grisard, E.; Buchrieser, J.; Schwartz, O.; Thery, C.; Lavieu, G. Quantitative characterization of extracellular vesicle uptake and content delivery within mammalian cells. *Nat. Commun.* **2021**, *12* (1), 1864.
(38) Shih, P.; Pedersen, L. G.; Gibbs, P. R.; Wolfenden, R. Hydrophobicities of the nucleic acid bases: distribution coefficients from water to cyclohexane. *J. Mol. Biol.* **1998**, *280* (3), 421−430.
(39) Rizzuto, F. J.; Dore, M. D.; Rafique, M. G.; Luo, X.; Sleiman, H. F. DNA Sequence and Length Dictate the Assembly of Nucleic Acid Block Copolymers. *J. Am. Chem. Soc.* **2022**, *144* (27), 12272−12279.
(40) Yu, L.; Xu, Y.; Al-Amin, M.; Jiang, S.; Sample, M.; Prasad, A.; Stephanopoulos, N.; Sulc, P.; Yan, H. CytoDirect: A Nucleic Acid Nanodevice for Specific and Efficient Delivery of Functional Payloads to the Cytoplasm. *J. Am. Chem. Soc.* **2023**, *145* (50), 27336−27347.
(41) Vanaja, S. K.; Russo, A. J.; Behl, B.; Banerjee, I.; Yankova, M.; Deshmukh, S. D.; Rathinam, V. A. K. Bacterial Outer Membrane Vesicles Mediate Cytosolic Localization of LPS and Caspase-11 Activation. *Cell* **2016**, *165* (5), 1106−1119.
(42) Dad, H. A.; Gu, T.-W.; Zhu, A.-Q.; Huang, L.-Q.; Peng, L.-H. Plant Exosome-like Nanovesicles: Emerging Therapeutics and Drug Delivery Nanoplatforms. *Mol. Ther.* **2021**, *29* (1), 13−31.
(43) Li, Y.; Zhao, R.; Cheng, K.; Zhang, K.; Wang, Y.; Zhang, Y.; Li, Y.; Liu, G.; Xu, J.; Xu, J.; Anderson, G. J.; Shi, J.; Ren, L.; Zhao, X.; Nie, G. Bacterial Outer Membrane Vesicles Presenting Programmed Death 1 for Improved Cancer Immunotherapy via Immune Activation and Checkpoint Inhibition. *ACS Nano* **2020**, *14* (12), 16698−16711.
(44) Timms, K.; Holder, B.; Day, A.; McLaughlin, J.; Forbes, K. A.; Westwood, M. Watermelon-Derived Extracellular Vesicles Influence Human Ex Vivo Placental Cell Behavior by Altering Intestinal Secretions. *Mol. Nutr. Food Res.* **2022**, *66* (19), No. e2200013.
(45) Yang, X.; Wen, X.; Dai, J.; Chen, Y.; Ding, W.; Wang, J.; Gu, X.; Zhang, X.; Chen, J.; Sutliff, R. L.; Emory, S. R.; Ruan, G. Probing the Intracellular Delivery of Nanoparticles into Hard-to-Transfect Cells. *ACS Nano* **2022**, *16* (6), 8751−8765.
(46) Buhrmann, C.; Busch, F.; Shayan, P.; Shakibaei, M. Sirtuin-1 (SIRT1) is required for promoting chondrogenic differentiation of mesenchymal stem cells. *J. Biol. Chem.* **2014**, *289* (32), 22048−22062.
(47) Warnecke, A.; Prenzler, N.; Harre, J.; Kohl, U.; Gartner, L.; Lenarz, T.; Laner-Plamberger, S.; Wietzorrek, G.; Staecker, H.; Lassacher, T.; Hollerweger, J.; Gimona, M.; Rohde, E. First-in-human

https://doi.org/10.1021/jacsau.4c00338
JACS Au 2024, 4, 2381−2392

intracochlear application of human stromal cell-derived extracellular vesicles. *J. Extracell. Vesicles* **2021**, *10* (8), No. e12094.
(48) Bertolino, G. M.; Maumus, M.; Jorgensen, C.; Noel, D. Therapeutic potential in rheumatic diseases of extracellular vesicles derived from mesenchymal stromal cells. *Nat. Rev. Rheumatol.* **2023**, *19* (11), 682−694.

https://doi.org/10.1021/jacsau.4c00338
JACS Au 2024, 4, 2381−2392